



Research
Drop-on-Demand Printing—Article

Multi-Objective Optimization Design through Machine Learning for Drop-on-Demand Bioprinting



Jia Shi ^{a,b}, Jinchun Song ^a, Bin Song ^c, Wen F. Lu ^{b,*}

^a School of Mechanical Engineering and Automation, Northeastern University, Shenyang 110819, China

^b Department of Mechanical Engineering, National University of Singapore, Singapore 119077, Singapore

^c Singapore Institute of Manufacturing Technology, Singapore 637662, Singapore

ARTICLE INFO

Article history:

Received 8 September 2018

Revised 1 December 2018

Accepted 25 December 2018

Available online 23 March 2019

Keywords:

Drop-on-demand printing

Inkjet printing

Gradient descent multi-objective optimization

Fully connected neural networks

ABSTRACT

Drop-on-demand (DOD) bioprinting has been widely used in tissue engineering due to its high-throughput efficiency and cost effectiveness. However, this type of bioprinting involves challenges such as satellite generation, too-large droplet generation, and too-low droplet speed. These challenges reduce the stability and precision of DOD printing, disorder cell arrays, and hence generate further structural errors. In this paper, a multi-objective optimization (MOO) design method for DOD printing parameters through fully connected neural networks (FCNNs) is proposed in order to solve these challenges. The MOO problem comprises two objective functions: to develop the satellite formation model with FCNNs; and to decrease droplet diameter and increase droplet speed. A hybrid multi-subgradient descent bundle method with an adaptive learning rate algorithm (HMSGDBA), which combines the multi-subgradient descent bundle (MSGDB) method with Adam algorithm, is introduced in order to search for the Pareto-optimal set for the MOO problem. The superiority of HMSGDBA is demonstrated through comparative studies with the MSGDB method. The experimental results show that a single droplet can be printed stably and the droplet speed can be increased from 0.88 to 2.08 m·s⁻¹ after optimization with the proposed method. The proposed method can improve both printing precision and stability, and is useful in realizing precise cell arrays and complex biological functions. Furthermore, it can be used to obtain guidelines for the setup of cell-printing experimental platforms.

© 2019 THE AUTHORS. Published by Elsevier LTD on behalf of Chinese Academy of Engineering and Higher Education Press Limited Company. This is an open access article under the CC BY-NC-ND license (<http://creativecommons.org/licenses/by-nc-nd/4.0/>).

1. Introduction

Inkjet printing is a cost-effective, fast, and versatile additive manufacturing technique. It is classified into continuous inkjet (CIJ) printing and drop-on-demand (DOD) printing, where DOD printing has wide applications in sensors [1], solar cells [2], memory devices [3], radio frequency devices [4], complex circuits [5], and tissue engineering [6,7]. DOD printing is popular because of its high accuracy, precision, and controllability for printing droplets. For example, it can be used in tissue engineering to place cells and biomaterials in specific target locations in order to achieve the necessary spatial resolution. Nevertheless, several adverse phenomena, including droplet satellites, large droplets, and slow droplet speed, can reduce printing precision, pattern

quality, controllability, and stability, hence restricting extensive application of inkjet printing [8].

During DOD bioprinting, there are three droplet statuses: no droplet, only primary droplet, and primary droplet with satellites [9,10]. “Only primary droplet” printing is the ideal printing result that can deposit cells in specific positions. Satellites are typically small droplets that are generated with the formation of the primary droplet. Satellite formation is mainly due to excessive droplet deformation caused by the Rayleigh instability [10]. Once the Bernoulli pressure generated by the speed is larger than the capillary force (generated by the surface tension) and viscous force, satellites are generated and decrease the printing precision and pattern quality.

Since DOD printing is usually used in micro-printing processes, droplet diameter is an important index for printing precision. Furthermore, very low droplet speed may cause the breakup of the droplet near the nozzle and generate a wet perimeter around the orifice of the nozzle. In bioprinting, cells in residual liquid

* Corresponding author.

E-mail address: mpelwlf@nus.edu.sg (W.F. Lu).

may adhere to the orifice of the nozzle, causing non-ideal wetting [11]. This phenomenon suppresses droplet formation and causes a non-straight flying trajectory, decreasing printing stability.

Droplet types, diameters, and speeds are influenced by printing parameters, such as the voltages applied in piezoelectric DOD printing, ink properties, and structure of the DOD print-head. It is difficult to describe the relationship between droplet features and printing parameters using a single physical model. Many researchers have focused on models that feature only one droplet with printing parameters for DOD printing. The main method is to study the generation and elimination models of satellites. Kim and Baek [12] have discussed the printability parameter range to produce a primary droplet without satellites using computational fluid dynamics (CFD) simulations. Dong et al. [9] have proposed a criterion for the maximal critical breakup length to avoid satellites. Poozesh et al. [13] have proposed a mechanism to generate various droplet sizes with no change in nozzle diameter, while satellites were generated.

Only a few studies have discussed a model that includes all of the above droplet features in order to optimize the DOD printing parameters, because these droplet features conflict with each other. For example, increasing droplet speed can enhance printing stability, but generates satellites. Reducing satellites or droplet diameter can improve printing precision, but may decrease droplet speed and printing stability. Thus, there is a need to find as good a solution as possible to balance these different goals through a multi-objective optimization (MOO) method.

Since no clear function model has been studied between droplet features and printing parameters, machine learning is herein proposed to map out this nonlinear and complex model. Machine learning has been proven to be effective in both classification and regression in many engineering fields [14–16]. Dos Santos et al. [17] used fully connected neural networks (FCNNs), a class of machine learning method, to build a model of the relation between printing parameters and droplet speed in pulsed gas metal arc welding. That work suggests that FCNNs work well in searching for a data relationship.

Many MOO methods have been proposed in the past, such as evolutionary methods [18,19] and descent methods [20]. Evolutionary methods use an evolutionary algorithm (EA), which is a generic population-based metaheuristic optimization algorithm. Candidate solutions to the optimization problem play the role of individuals in a population, and the fitness function determines the quality of the solutions. Descent methods use a gradient descent algorithm, which is a first-order iterative optimization algorithm. To find the local minimum of a function using gradient

descent, steps are taken proportional to the negative of the gradient (or approximate gradient) of the function at the current point. FCNNs have more complex function structures than common functions because they may have several hidden layers. Optimizing FCNNs with EAs may not achieve a Pareto-efficient set, since there are no common convergence criteria. Instead, descent methods rely on rigorous convergence theorems and can achieve calculation stability.

To solve the problems of low printing precision and stability caused by satellites and a slow printing speed, we propose an efficient MOO design method for optimizing piezoelectric DOD printing parameters. Fig. 1 shows a schematic diagram of the proposed method. Both single-objective optimization (SOO) and MOO problems are built to optimize the DOD printing parameters, and FCNNs are used to identify the relationship between satellite formation and printing parameters. The simulation model in our previous work is used to collect datasets for the FCNNs due to its convenience and accuracy [21]. The SOO problem, which is solved by the Adam algorithm, simulates the case of reducing satellite formation with the use of a fixed print-head and bio-ink. The MOO problem simulates the case of building an experimental platform for optimal printing. A hybrid multi-subgradient descent bundle method with an adaptive learning rate algorithm (HMSGDBA) is proposed, which combines the multiple subgradient descent bundle (MSGDB) method with the Adam algorithm to solve the MOO problem. Our experiments verify that a single droplet with a smaller droplet diameter can be printed and a faster speed can be realized using the proposed method, thus improving the printing precision and stability.

2. Methodology

This section firstly presents a brief description of DOD printing and satellite formation, then discusses the FCNNs model of satellites formation and the optimal design problem of DOD printing parameters as well as the algorithms used in this paper, and finally introduces our experimental setup.

2.1. Models of piezoelectric DOD printing and satellite formation

In this section we address models of piezoelectric DOD printing, which combines inverse piezoelectric effect and compressible fluid theory, and the satellite formation defined according to the degree of droplet deformation.

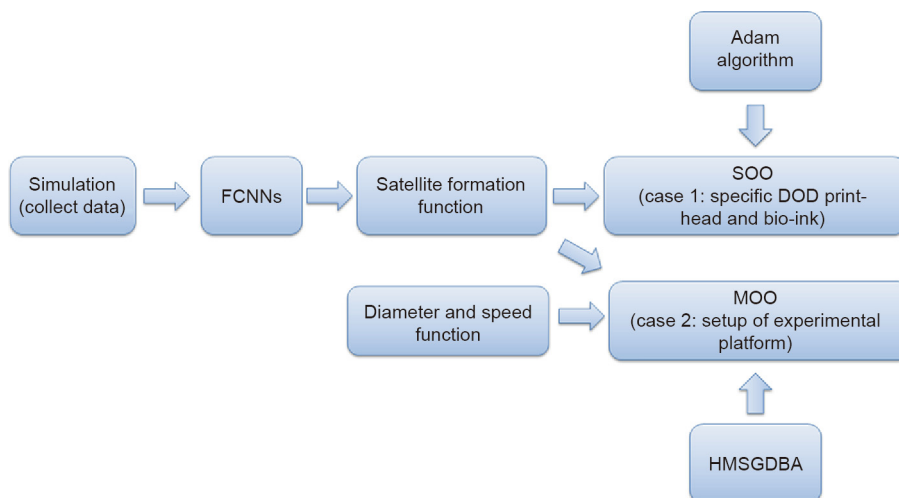


Fig. 1. Schematic diagram of the proposed method.

2.1.1. Models of piezoelectric DOD printing

In piezoelectric DOD printing, a transient mechanical pulse is applied to the fluid in the print-head by a piezoelectric actuator based on the inverse piezoelectric effect. This causes the bio-ink to be extruded through the nozzle, producing droplets as shown in Fig. 2. At each pulse cycle, a voltage is applied to the piezoelectric ceramic tube of the print-head to deform the tube wall. The deformation causes transient changes in the internal fluid volume in order to generate a pressure to produce droplets, according to the compressible fluid theory. The inverse piezoelectric effect, which includes compressible fluid theory, is expressed as follows:

$$\varepsilon = d_{33}U \quad (1)$$

$$\frac{\Delta V}{V} = \frac{\varepsilon}{r} \quad (2)$$

$$\Delta p = -K \frac{\Delta V}{V} \quad (3)$$

where ε is the deformation displacement of the tube along the thickness direction (m); d_{33} is the piezoelectric strain constant of PZT-5H, the piezoelectric ceramics based on BaTiO₃, $593 \times 10^{-12} \text{ m}\cdot\text{V}^{-1}$; U is the applied voltage (V); ΔV is the change of fluid volume (m³); V is initial volume of fluid (m³); Δp is the pressure variation (Pa); and K is the bulk modulus of elasticity of the fluid, $2.18 \times 10^9 \text{ Pa}$.

The continuity equation (Eq. (4)) and the Navier–Stokes equation (Eq. (5)), along with Eqs. (1)–(3), form a complete mathematical description of piezoelectric DOD printing and droplet formation:

$$\frac{\partial \rho}{\partial t} + \nabla \cdot (\rho \mathbf{u}) = 0 \quad (4)$$

$$\frac{\partial}{\partial t} (\rho \mathbf{u}) + \nabla \cdot (\rho \mathbf{u} \mathbf{u}) = -\nabla p + \nabla \cdot [\mu (\nabla \mathbf{u} + \nabla \mathbf{u}^T)] + \mathbf{f}^\sigma \quad (5)$$

where ρ is the density of fluid (kg·m⁻³), \mathbf{u} is the velocity (m·s⁻¹), μ is the viscosity of fluid (kg·m⁻¹·s⁻¹), and \mathbf{f}^σ is the surface tension force (N).

The surface tension force \mathbf{f}^σ in Eq. (5) is expressed based on the continuum surface force model as follows [22]:

$$\mathbf{f}_i^\sigma = -\sigma \frac{\bar{\rho} \nabla \cdot \frac{\alpha_j}{|\alpha_j|} \nabla \alpha_i}{\frac{1}{2}(\rho_i + \rho_j)} \quad (6)$$

where σ is the surface tension of bio-ink (N·m⁻¹), $\bar{\rho}$ is the volume-averaged density (kg·m⁻³), ρ_i is the density of the current

calculated phase in fluid (kg·m⁻³), ρ_j is the density of the other phase in the fluid (kg·m⁻³), α_i is the volume of the current calculated phase in the fluid, and α_j is the volume of the other phase in the fluid.

$\bar{\rho}$ is calculated with the volume-of-fluid model as follows [23]:

$$\bar{\rho} = (1 - \rho_i)\rho_j + \alpha_i\rho_i \quad (7)$$

2.1.2. Models of satellite formation

Taylor [24] proposed the use of a dimensionless number D in Eq. (8) to define the degree of droplet deformation:

$$D = C_a \frac{19\beta + 16}{16\beta + 16} \quad (8)$$

where D is the dimensionless number of droplet deformation, C_a is the capillary number, β and is the ratio of droplet viscosity to air viscosity.

C_a is expressed as follows:

$$C_a = \frac{\mu_l R_d \dot{\gamma}}{\sigma} \quad (9)$$

where μ_l is the viscosity of bio-ink (m·s⁻¹), R_d is the radius of droplet (m), and $\dot{\gamma}$ is the shear rate of the cell-laden bio-ink (s⁻¹).

D is selected as the evaluation index of the droplet status. The relation between droplet status y and D is expressed as follows:

$$y = \begin{cases} \text{No droplet,} & D = 0 \\ \text{Primary droplet,} & s \leq D \leq l \\ \text{Satellites,} & D > l \end{cases} \quad (10)$$

where s and l are the lower and upper boundary of D , respectively.

According to the mathematical model of DOD printing, the values of the Bernoulli pressure, capillary pressure, viscosity pressure, and unsteady pressure are determined by the applied voltage U , viscosity μ_1 and surface tension σ of the bio-ink, and nozzle diameter of the print-head D_n . Droplet deformation is expressed as a function of the printing parameters as follows:

$$D = f(U, \mu_1, \sigma, D_n) \quad (11)$$

CFD simulations can simulate the piezoelectric DOD printing process as well as satellite formation [21], thus helping researchers to comprehend the working principles of DOD printing. However, this method cannot obtain a precise mathematical model of Eq. (11) because of its complexity. Thus, we select the FCNN method to fit this function, and use CFD simulations to collect training datasets (Fig. 1).

2.2. Optimization design of DOD printing parameters

An optimization design of the DOD printing parameters can improve the printing performance and allow high precision and high stability. FCNNs are first developed to build a model of satellite formation; next, the optimization design is conducted in two cases, as shown in Fig. 1. The first case is an SOO of the applied voltage with the specific DOD print-head and bio-ink. The second case is an MOO design of all the printing parameters to obtain the optimal printing result.

2.2.1. FCNN model of satellite formation

FCNNs have three types of layers (Fig. 3): the input layer, hidden layers, and the output layer. The parameters to be analyzed constitute the input layer, and the fitted result is exported by the output layer. The middle hidden layers establish the nonlinear model of satellite formation, and can be one or many in number. The different layers are connected by weights and biases.

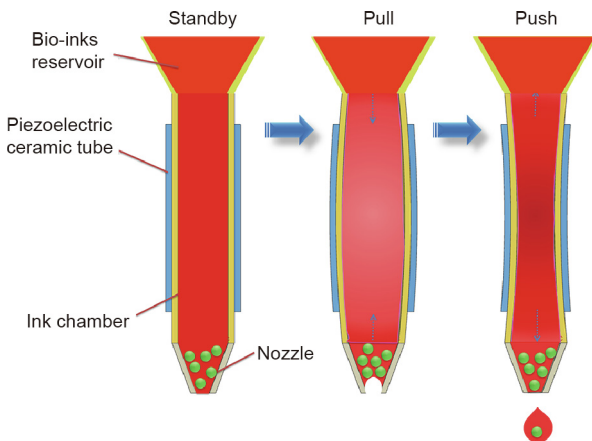


Fig. 2. Schematic of the piezoelectric DOD print-head.

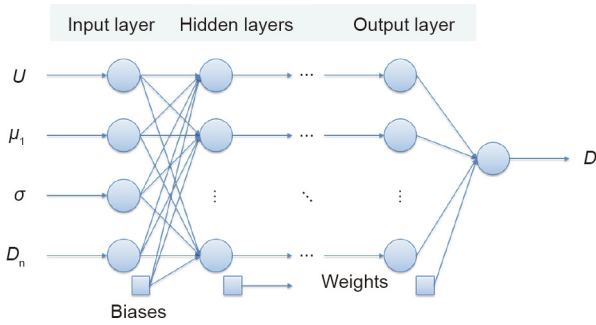


Fig. 3. Schematic diagram of FCNNs.

Since the function in Eq. (11) is piecewise continuous, the hidden layers in the FCNNs should be set as either a minimum of two layers comprising smooth activation functions, or one layer comprising both smooth and nonsmooth activation functions, in order to obtain satisfactory fitting results [25,26]. Here, the nonsmooth activation function is selected as the ReLU activation function, defined as rectified linear units, because of its sparse activation, which is beneficial in fitting the first part of the function $D = f(U, \mu_1, \sigma, D_n)$ —that is, $D = 0$, corresponding to the “no droplet” status. Three structures of hidden layers were designed to achieve the best fitting accuracy. The first is composed of one hidden layer with two activation functions—that is, the sigmoid and ReLU activation functions, where the ReLU activation function is nonsmooth. The second comprises two hidden layers with one activation function each—that is, the ReLU and tanh activation functions. The last includes two hidden layers with three activation functions, where the first hidden layer combines the sigmoid and ReLU activation functions, and the second layer is comprised of the tanh activation function. The activation functions are expressed in Eq. (12):

$$\begin{aligned}
 \text{Sigmoid : } & f(x) = 1/(1 + e^{-x}) \\
 \text{ReLU : } & f(x) = \begin{cases} x, & \text{if } x \geq 0 \\ 0, & \text{if } x < 0 \end{cases} \\
 \text{Tanh : } & f(x) = (1 - e^{-2x})/(1 + e^{-2x})
 \end{aligned} \tag{12}$$

The results of the CFD simulations were obtained as datasets for the FCNNs [21]. A total of 120 results were obtained, of which 87 were used as training sets and 33 as test sets. In the inputs of the datasets, the range of voltage was 15–54 V; the range of viscosity was 1.07–10 cP (1 cP = 10^{-3} Pa·s); the range of surface tension was 40–72.19 mN·m⁻¹; and the range of the nozzle diameter was 25–120 μm. The ranges of the voltage and viscosity were set according to the working scope of our DOD print-head, the range of the surface tension was set based on the common cell concentrations of bio-inks [11], and the range of the nozzle diameter was set larger than the diameter of the cells commonly used for bioprinting. Each input set was selected to train the FCNNs by sufficient different droplet statuses. As listed in Table 1, the values of D were around 10^{-8} – 10^{-7} with the prepared bio-inks described in Section 2.4. The outputs of the datasets were set as values of D magnified 10^6 times in order to improve the fitting accuracy. The Adam algorithm introduced in Section 2.3 was used to train the FCNNs. Three optimal FCNNs were obtained by optimizing

Table 1
Values of D to print primary droplet in experiments.

Boundary	Bio-ink		
	A	B	C
s	2.39×10^{-8}	2.13×10^{-8}	2.03×10^{-8}
l	5.88×10^{-8}	5.86×10^{-8}	4.80×10^{-8}

Table 2
Structures of the designed FCNNs and test results.

FCNN	Parameters			MAE	RMSE
	Nodes	l_r^a	Epochs		
1	5; 1	0.005	20 000	10.9%	13.9%
2	9; 2	0.008	30 000	9.9%	13.4%
3	2; 2; 2	0.012	20 000	9.4%	10.9%

^a l_r represents the learning rate used in the Adam algorithm to train FCNNs.

the parameters of the FCNNs, including the numbers of hidden nodes, learning rate, and training epochs. Their structures and the test results are listed in Table 2. The third FCNN had the best test accuracy, with a least mean absolute error (MAE) of 9.4% and a least root mean squared error (RMSE) of 10.9%. This FCNN was set as the model of satellite formation in Eq. (11).

2.2.2. Single-objective optimization design of voltages

In the first case, both the piezoelectric DOD print-head and the bio-ink are specified. The applied voltage is the only parameter to be adjusted, in order to reduce satellite formation. The design of the DOD printing parameters is treated as a SOO problem, as follows:

$$\begin{aligned}
 \text{Objective : } & \min \frac{1}{2} [f(U) - c_1 c_2 D_0]^2 \\
 \text{Subject to : } & U \in [15, 54]
 \end{aligned} \tag{13}$$

where D_0 is the specific value of D that refers to the condition of printing a primary droplet without satellites; c_1 and c_2 are the correction coefficients, $c_1 = 0.89$ and $c_2 = 0.90$. The Adam algorithm is used to solve this optimization problem.

D_0 is determined through experiments according to the boundary of D (Table 1)—that is, s and l in Eq. (10). The experimental setup and the three cell-laden bio-inks used in the experiments are described in Section 2.4. The boundaries of D are listed in Table 1, which lists the maximum of s , named s_{\max} , as 2.39×10^{-8} and the minimum of l , named l_{\min} , as 4.80×10^{-8} . Printing only primary droplets can be guaranteed when D belongs to $[s_{\max}, l_{\min}]$. Here, D_0 is set as a median value between s_{\max} and l_{\min} —that is, 3.3×10^{-8} —as the objective value of D .

Two correction coefficients, c_1 and c_2 , are set to reduce the error among the experiments, FCNNs, and simulation results. Simulation errors in the droplet radius and droplet speed are almost 7% and 4%, respectively [21], and c_1 is thus set as 0.89. The FCNN error is 9.4% and c_2 is set as 0.90.

2.2.3. Multi-objective design optimization of DOD printing parameters

In the second case, the setup of a bioprinting experimental platform requires suitable and cost-effective DOD print-heads and bio-inks. Thus, all the printing parameters require optimization. The platform is expected to satisfy several requirements in addition to satellite reduction, such as high printing precision and a robust and easy printing process. These requirements can be realized by decreasing the diameter of the nozzle, increasing the printing speed by amplifying the applied voltage, and selecting a bio-ink with low viscosity and low surface tension. However, these demands conflict with the demand of reducing satellite formation [9]. Under this condition, the design of the DOD printing parameters is considered to be an MOO problem, as follows:

$$\begin{aligned}
 \text{Objective : } & f_1 = \min [0.1 \times (\mu_1' + \sigma' + D_n' - U')] \\
 & f_2 = \min \left\{ \frac{1}{2} [f(U, \mu_1, \sigma, D_n) - c_1 c_2 D_0]^2 \right\} \\
 \text{Subject to : } & U \in [15, 54] \\
 & \mu_1 \in [1, 10] \\
 & \sigma \in [40, 72.19] \\
 & D_n \in [25, 100]
 \end{aligned} \tag{14}$$

In the MOO model, f_1 represents the goal of increasing printing precision and stability, while f_2 represents the goal of avoiding satellite formation. The coefficient of 0.1 in f_1 balances the effect of functions f_1 and f_2 . U' , μ'_i , σ' , and D'_n normalize the parameter according to their range as follows:

$$x' = \frac{x - (x_{\max} + x_{\min})/2}{(x_{\max} - x_{\min})/2} \quad (15)$$

2.3. Multi-objective optimization with the descent method

FCNNs are powerful models with non-convex objective functions that have very complex function structures. At first, we tried using an evolutionary MOO algorithm called the multi-objective particle swarm optimization (MOPSO) [27] to optimize Eq. (14); however, the result was non-convergent. Even though descent-based MOO algorithms have a slower numerical calculation speed than many evolutionary MOO algorithms, we selected them to solve the presented problem due to their rigorous convergence theorems. The HMSGDBA is hence proposed, which combines the MSGDB method with the Adam algorithm, in order to solve our MOO problem.

2.3.1. The multiple subgradient descent bundle method

The MSGDB method is a gradient descent-based method for convex nonsmooth MOO problems [28]. It uses the proximal bundle approach first to find descent directions for each objective function, considering the nonsmoothness features. A convex hull of these descent directions is formed, and the minimum norm element is then calculated as a candidate of the common descent direction for all objective functions. If a common descent direction is not found, the union of subdifferentials of the objectives is approximated instead of the above descent directions. This method can at least converge to a weak Pareto-optimal set. The steps of the MSGDB method are as follows:

(1) Initialization: Randomly select the starting point \mathbf{x}_1 ; set the stopping parameter $\varepsilon_m > 0$.

(2) Find the direction \mathbf{d}_{ii} for all numbers of the objective junctions $ii = 1, \dots, m$ separately with an inner iteration kk as follows:

$$\mathbf{d}_{ii,kk} = \operatorname{argmin} \left\{ \hat{f}_{ii}^{kk}(\mathbf{x}_{kk} + \mathbf{d}_{ii}) + \frac{1}{2} \mathbf{d}_{ii}^2 \mid \mathbf{d}_{ii} \in \mathbf{R}^n \right\} \quad (16)$$

where $\hat{f}_{ii}^{kk}(\mathbf{x})$ is a piecewise linear model to approximate the function f_{ii} [29], set $\mathbf{d}_{ii} = \mathbf{d}_{ii,kk}$.

(3) Calculate a minimum norm element as the common descent direction \mathbf{d}_{ii} by solving the following:

$$\begin{aligned} \text{Objective : } & \min \left\| \sum_{ii=1}^m \lambda_{ii} \mathbf{d}_{ii} \right\|^2 \\ \text{Subject to : } & \sum_{ii=1}^m \lambda_{ii} = 1 \\ & \lambda_{ii} \geq 0 \end{aligned} \quad (17)$$

(4) If $f_{ii}(\mathbf{x}_{ii} + \mathbf{d}_{ii}) < f_{ii}(\mathbf{x}_{ii})$, go to step (6). Otherwise, go to step (5). If $\|\mathbf{d}_{ii}\| < \varepsilon_m$, then stop.

(5) Use the proximal bundle method to build a set of subgradients and find another candidate of the common descent direction [29].

(6) Update the parameters with a line-searched step size τ :

$$\mathbf{x}_{ii+1} = \mathbf{x}_{ii} + \tau \mathbf{d}_{ii} \quad (18)$$

2.3.2. Adaptive moment estimation

The adaptive moment estimation (i.e., Adam algorithm) is a first-order gradient-based optimization algorithm of the stochastic objective function, which is computationally efficient, requests

little memory, and is invariant to diagonal rescaling of the gradients [30]. It computes the individual adaptive learning rate for different parameters from estimates of the first and second moments of gradients. The method has been proven to be effective and is widely applied in training the weights matrices of deep learning networks [31]. This study used Adam algorithm to ① optimize the weights matrices of the designed FCNNs and ② generate updated steps in the proposed HMSGDBA. The core steps of Adam algorithm are summarized as follows:

(1) Initialization: $f(\theta)$ is the objective function with parameters θ ; θ_0 is the initial weights and bias matrix of the designed FCNNs; the initialized time step is $t = 0$; the learning rate $\eta = 0.012$; and the other initialized parameters are $m_0 = 0$, $v_0 = 0$, $\beta_1 = 0.9$, $\beta_2 = 0.999$, and $\varepsilon = 10^{-8}$.

(2) Obtain gradients with respect to the objective function at time step t :

$$\mathbf{g}_t = \nabla_{\theta} f_t(\theta_{t-1}) \quad (19)$$

(3) Update the biased first moment and second raw moment:

$$\mathbf{m}_t = \beta_1 \cdot \mathbf{m}_{t-1} + (1 - \beta_1) \cdot \mathbf{g}_t \quad (20)$$

$$\mathbf{v}_t = \beta_2 \cdot \mathbf{v}_{t-1} + (1 - \beta_2) \cdot \mathbf{g}_t^2 \quad (21)$$

where \mathbf{g}_t^2 indicates the elementwise square $\mathbf{g}_t \odot \mathbf{g}_t$.

(4) Compute the bias-corrected first moment and second raw moment:

$$\hat{\mathbf{m}}_t = \mathbf{m}_t / (1 - \beta_1^t) \quad (22)$$

$$\hat{\mathbf{v}}_t = \mathbf{v}_t / (1 - \beta_2^t) \quad (23)$$

(5) Update the parameters:

$$\theta_t = \theta_{t-1} - \eta \cdot \hat{\mathbf{m}}_t / (\sqrt{\hat{\mathbf{v}}_t} + \varepsilon) \quad (24)$$

(6) If the convergence conditions are satisfied, the resulting parameters θ_t are returned; otherwise, go back to step (2).

2.3.3. The hybrid multi-subgradient descent bundle method with the adaptive learning rate algorithm

The MSGDB method may be unsuitable for optimizing the objective function of non-convex FCNNs due to the possibility of falling into a local optimum, while Adam outperforms other methods in such cases because it performs a form of step-size annealing and is able to jump out of the local optimum and be infinitely close to the global optimum [30]. HMSGDBA is hence designed to combine the advantages of MSGDB method and Adam algorithm in order to ensure convergence and calculation stability. In HMSGDBA, the common descent direction for all the objective functions is found using MSGDB, and the inputs parameters are updated by Adam algorithm with a learning rate of 0.001 along the found direction. The convergence conditions are set as $\|\mathbf{d}_{ii}\| < \varepsilon_m$. Since the solution of an MOO problem with a gradient descent algorithm is sensitive in terms of starting points, several starting points are selected in order to obtain a Pareto-optimal set.

2.4. Experimental setup

An in-house-developed piezoelectric DOD print-head with a nozzle diameter of 100 μm was used in this study (Fig. 4). A high-speed camera (Mini AX200 model, Photron), assisted by a super-bright light emitting diode (LED) (SLG-150V, REVOX Solutions by Photron), was used to capture the droplet trajectory at a frame rate of 40 000. The camera was focused on the middle plane of the nozzle, and the droplet formation process was recorded. The voltage pulse was applied to a piezo driver (JetDrive™ III,

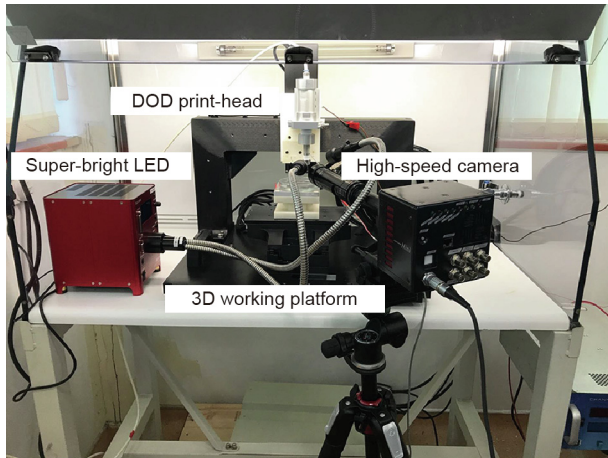


Fig. 4. Experimental setup for piezoelectric DOD cell printing. 3D: three-dimensional.

MicroFab Technologies Inc.) to produce droplets. The piezo driver was connected with the transducer of the print-head.

Three kinds of cell-laden bio-inks were used to test the SOO results (Table 3) [21]. These comprised HeLa cells and Dulbecco's Modified Eagle Medium (DMEM), or sodium alginate (SA) dissolved in DMEM, to obtain different viscosities. When increasing the concentration of SA to 1.0%, two cell concentrations, 1×10^6 and $5 \times 10^5 \text{ mL}^{-1}$, were initially used. The testing results showed that both had almost the same viscosity, while the one with $1 \times 10^6 \text{ mL}^{-1}$ cells could not break into droplets after ejection. A possible reason for this result is that the surface tension value of this bio-ink decreases during the transient process of generating droplets, which reduces the total free energy and increases the printing difficulty [11]. Hence, cells with a concentration of $5 \times 10^5 \text{ mL}^{-1}$ were selected for the preparation of bio-ink C as listed in Table 3 in order to ensure that the printer was working well.

3. Results and discussion

Experiments were conducted to verify that the proposed method could be used to obtain stable and precise printing results. The optimization results introduce a guideline for the design of a DOD print-head.

3.1. Verification of voltage optimization results

In the SOO problem, the applied voltage was optimized to print only primary droplets with the bio-inks listed in Table 3. The initial voltage was randomly set at 40 V. Table 4 lists the droplet status under the initial voltages and the optimized voltages for each bio-ink. The experimental results showed that printing bio-inks A and B with the initial voltage generated satellites, while printing bio-ink C with the initial voltage did not generate droplets. All of the optimized voltages were able to generate only primary droplets when printed with the corresponding bio-ink (Fig. 5), which verified the designed FCNNs and the SOO results.

Table 3
Properties of cell-laden bio-inks.

Bio-ink	DMEM	SA concentration (w/v)	Cell concentration (mL^{-1})	Viscosity (cP)	Surface tension ($\text{mN}\cdot\text{m}^{-1}$)
A	Yes	0	1×10^6	1.07	72.19
B	Yes	0.5%	1×10^6	5.00	71.00
C	Yes	1.0%	5×10^5	10.00	70.03

Given a specific bio-ink and DOD print-head, the applied voltage could be designed to print only primary droplets. This method can replace the trial-and-error process of cell printing experiments and can thus save researchers the expense of obtaining instruments for observing droplet statuses, such as high-speed cameras and microscopes.

3.2. Optimization design of DOD printing parameters

In the MOO problem, based on the verified FCNNs, all the printing parameters were optimized by solving Eq. (14). A Pareto-optimal set was obtained using HMSGDBA and MSGDB (Fig. 6). The results show that HMSGDBA achieves a Pareto set that is closer to the global optimum than the results obtained using MSGDB.

According to the results for HMSGDBA shown in Fig. 6, the maximum error of f_2 is greater than 2×10^{-3} when f_1 is at the minimal value of -0.4 . The corresponding D is around 1.121×10^{-7} , which indicates that satellites will be printed. The value of f_2 decreases with an increasing value of f_1 . At the labeled point in the figure, f_2 is 6.12×10^{-6} and f_1 is -0.14 . This condition is ideal for printing only primary droplets in a stable manner. Although increasing f_1 could further decrease f_2 , the printing precision and stability might worsen. The labeled point can hence be treated as a compromise solution. Table 5 lists the initial, optimized, and adjusted values of the printing parameters. It demonstrates that satellites can be printed initially with D of 8.84×10^{-8} . After optimization, only primary droplets are printed with a D of 3.75×10^{-8} , and the printing precision and stability are improved with a decrease in f_1 . Consequently, the optimal set of printing parameters is 39 V, 1.37 cP, $65.91 \text{ mN}\cdot\text{m}^{-1}$ and $29 \mu\text{m}$. According to the common properties of the bio-ink and the nozzle diameter of the piezoelectric DOD print-head, the printing parameters are adjusted with a D of 3.77×10^{-8} . The optimized bio-ink can be prepared by adding surfactants to bio-ink A [32]. The small difference between the adjusted D and the optimal D can be omitted because it has no influence on the final printing results.

Table 4
The droplet status under the initial voltages and the optimized voltages for cell-laden bio-inks.

		Bio-ink		
		A	B	C
Initial	Voltage (V)	40	40	40
	Droplet status	Satellites	Satellites	No droplet
Optimized	Voltage (V)	29	35	43
	Droplet status	Single	Single	Single
	Time to output after optimized (μs)	550	575	575

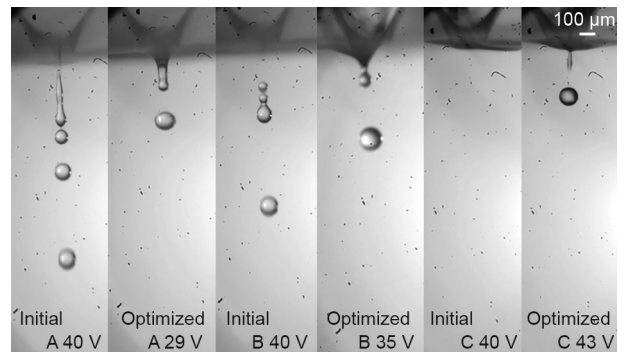


Fig. 5. Experiments printing different bio-inks with optimized voltages.

Due to the limitation of our DOD print-head, the proposed method was verified with a fixed nozzle diameter of 100 μm . The initial printing condition used bio-ink B with an applied voltage of 33 V. Even though a single droplets without satellites was printed at first, as shown in Fig. 7(a), no droplets were generated after several moments due to the generation of a wet perimeter caused by a slow droplet speed of 0.88 $\text{m}\cdot\text{s}^{-1}$. Using the proposed method, the printing parameters were optimized for applied voltage, viscosity, and surface tension as 20 V, 1.05 cP, and 41 $\text{mN}\cdot\text{m}^{-1}$, respectively. The designed bio-ink was prepared by mixing 0.01% w/v fluorosurfactant Novec FC-4430 with bio-ink A [32], and the viscosity and the surface tension of the prepared bio-ink are 1.07 cP, and 41.5 $\text{mN}\cdot\text{m}^{-1}$. The small error of viscosity and surface tension between the designed and prepared bio-ink was ignored. The results showed that single droplets were printed stably with the prepared bio-ink (Fig. 7(b)) at a printing speed of 2.08 $\text{m}\cdot\text{s}^{-1}$. A video of the printing process shown in Fig. 7 is provided in the Appendix A.

Considering that the DOD print-head is usually fixed, Eq. (14) was adjusted to determine suitable properties of bio-ink for different biological functions. The optimal value of f_1 was set as -0.15 and the nozzle diameter was set as a constant for the best printing precision stability. The new objectives are expressed as follows:

$$\begin{aligned} \text{Objective: } f_1 &= \min\{[0.1 \times (\mu_1' + \sigma' + D_n' - U') + 0.15]^2\} \\ f_2 &= \min\left\{\frac{1}{2}[f(U, \mu_1, \sigma, D_n) - c_1 c_2 D_0]^2\right\} \\ \text{Subject to: } U &\in [15, 54] \\ \mu_1 &\in [1, 10] \\ \sigma &\in [40, 72.19] \\ D_n &\equiv 30 \end{aligned} \quad (25)$$

The solutions of Eq. (25) illustrate that a satisfactory viscosity of bio-ink is from 1.00 to 2.60 cP, surface tension is from 50.35 to

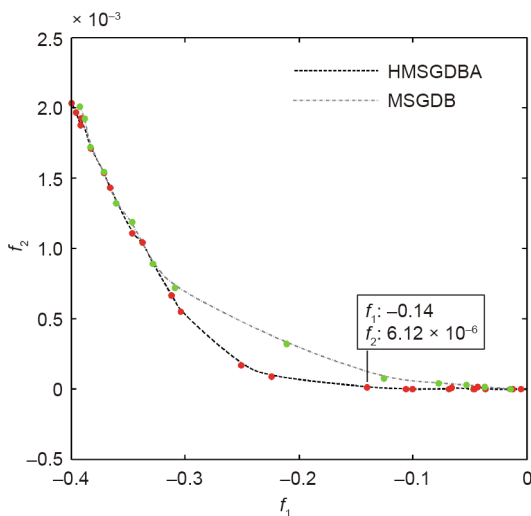


Fig. 6. Solutions obtained in objective space for the optimization design of DOD printing parameters using HMSGDBA and MSGDB.

Table 5
Comparison of printing performance with different printing parameters.

	U (V)	μ_1 (cP)	σ ($\text{mN}\cdot\text{m}^{-1}$)	D_n (μm)	f_1	f_2 ($\times 10^{-6}$)	D ($\times 10^{-8}$)
Initial	51	6.12	72.00	59	0.19	981.20	8.84
Optimized	39	1.37	65.91	29	-0.14	6.12	3.75
Adjusted	39	1.07	66.00	30	-0.15	6.84	3.77

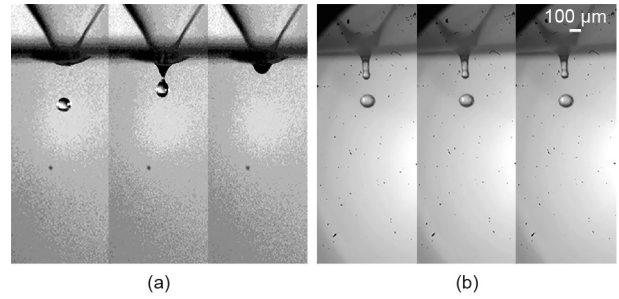


Fig. 7. Experimental validation of the proposed method. (a) Experimental results with the initial printing parameters of $U = 33$ V, $\mu_1 = 5$ cP, and $\sigma = 71.00$ $\text{mN}\cdot\text{m}^{-1}$; (b) experimental results with the optimized printing parameters of $U = 20$ V, $\mu_1 = 1.07$ cP, and $\sigma = 41.5$ $\text{mN}\cdot\text{m}^{-1}$.

67.55 $\text{mN}\cdot\text{m}^{-1}$, and corresponding voltage is from 22 to 40 V. These results imply that printing a bio-ink with high viscosity, such as a high-concentration hydrogel, cannot yield the best printing precision with a robust printing process. The computed range for the viscosity and surface tension of bio-ink can be treated as a reference for the preparation of bio-ink.

4. Conclusions

This paper proposed an effective multi-objective design optimization method for optimizing piezoelectric DOD printing parameters to print droplets with a smaller droplet diameter and faster droplet speed, without satellites. SOO and MOO problems were solved through FCNNs in order to optimize the DOD printing parameters. FCNNs including two hidden layers with a nonsmooth activation function were verified as having the best accuracy. The experiments demonstrated that an optimized voltage for each bio-ink, obtained by solving the SOO problem, can be used to print single primary droplets successfully. The MOO problem was solved by the proposed HMSGDBA, which combines MSGDB with the Adam algorithm. The obtained approximation of the Pareto set was closer to the global solution than the results obtained using MSGDB. Compared with non-optimized initial printing parameters, the optimized parameters obtained by the proposed method were able to improve the printing precision and stability. Experiments were conducted to validate the SOO and MOO method with a fixed nozzle of 100 μm . The results showed that single droplets were stably printed after optimization in the SOO problem. In the MOO problem, the droplet speed was increased from 0.88 to 2.08 $\text{m}\cdot\text{s}^{-1}$ after optimization. Furthermore, based on the optimized nozzle diameter of the DOD print-head, a range of bio-ink properties was proposed as a reference for preparing bio-ink to obtain the best printing precision with a robust printing process. The suggested bio-ink viscosity is from 1.00 to 2.60 cP, the surface tension is from 50.35 to 67.55 $\text{mN}\cdot\text{m}^{-1}$, and the corresponding voltage is from 22 to 40 V. The proposed method improves the printing precision and stability for precise order of cell arrays. Optimized results can be treated as a guideline for the setup of a piezoelectric DOD bioprinting experimental platform.

Acknowledgement

This work was supported by the China Scholarship Council (CSC) (2016080037).

Compliance with ethics guidelines

Jia Shi, Jinchun Song, Bin Song, and Wen F. Lu declare that they have no conflict of interest or financial conflicts to disclose.

Nomenclature

ε	deformation displacement of the tube along the thickness direction (m)
d_{33}	piezoelectric strain constant of PZT-5H, the piezoelectric ceramics based on BaTiO ₃ , $593 \times 10^{-12} \text{ m}\cdot\text{V}^{-1}$
U	applied voltage (V)
ΔV	change of fluid volume (m ³)
V	initial volume of fluid (m ³)
r	inner diameter of piezoelectric ceramic tube (m)
Δp	pressure variation (Pa)
K	bulk modulus of elasticity of the fluid, $2.18 \times 10^9 \text{ Pa}$
ρ	density of fluid (kg·m ⁻³)
\mathbf{u}	velocity (m·s ⁻¹)
p	static pressure (Pa)
μ	viscosity of fluid (kg·(m·s) ⁻¹)
\mathbf{f}^σ	surface tension force (N)
\mathbf{f}_i^σ	surface tension force of the current phase
σ	surface tension of bio-ink (N·m ⁻¹)
$\bar{\rho}$	volume-averaged density (kg·m ⁻³)
ρ_i	density of the current calculated phase in fluid (kg·m ⁻³)
ρ_j	density of the other phase in the fluid (kg·m ⁻³)
α_i	volume of the current calculated phase in the fluid
α_j	volume of the other phase in the fluid
D	dimensionless number of droplet deformation
μ_l	viscosity of bio-ink (m·s ⁻¹)
R_d	radius of droplet (m)
s	lower boundary of D
l	upper boundary of D
C_a	capillary number, a dimensionless number
β	ratio of droplet viscosity to air viscosity
γ	shear rate of the liquid, i.e., cell-laden bio-ink (s ⁻¹)
D_n	nozzle radius of DOD print-head (m)
c_1, c_2	correction coefficients: $c_1 = 0.89, c_2 = 0.90$

Appendix A. Supplementary data

Supplementary data to this article can be found online at <https://doi.org/10.1016/j.eng.2018.12.009>.

References

- [1] Su W, Tentzeris MM. Smart test strips: next-generation inkjet-printed wireless comprehensive liquid sensing platforms. *IEEE Trans Ind Electron* 2017;64(9):7359–67.
- [2] Jung S, Sou A, Banger K, Ko DH, Chow PC, McNeill CR, et al. All-inkjet-printed, all-air-processed solar cells. *Adv Energy Mater* 2014;4(14):1400432.
- [3] Rajan K, Bocchini S, Chiappone A, Roppolo I, Perrone D, Castellino M, et al. WORM and bipolar inkjet printed resistive switching devices based on silver nanocomposites. *Flexible Printed Electronics* 2017;2(2):024002.
- [4] Chiolerio A, Camarchia V, Quaglia R, Pirola M, Pandolfi P, Pirri CF. Hybrid Ag-based inks for nanocomposite inkjet printed lines: RF properties. *J Alloys Compound* 2014;615:S501–4.
- [5] Zheng Y, He Z, Gao Y, Liu J. Direct desktop printed-circuits-on-paper flexible electronics. *Sci Rep* 1786;2013:3.
- [6] Wang K, Ho CC, Zhang C, Wang B. A review on the 3D printing of functional structures for medical phantoms and regenerated tissue and organ applications. *Engineering* 2017;3(5):653–62.
- [7] Liu Y, Zhou G, Cao Y. Recent progress in cartilage tissue engineering—our experience and future directions. *Engineering* 2017;3(1):28–35.
- [8] Pereira F, Bártolo PJ. 3D photo-fabrication for tissue engineering and drug delivery. *Engineering* 2015;1(1):90–112.
- [9] Dong H, Carr WW, Morris JF. An experimental study of drop-on-demand drop formation. *Phys Fluids* 2006;18(7):072102.
- [10] Yang Q, Li H, Li M, Li Y, Chen S, Bao B, et al. Rayleigh instability-assisted satellite droplets elimination in inkjet printing. *ACS Appl Mater Interfaces* 2017;9(47):41521–8.
- [11] Xu C, Zhang M, Huang Y, Ogale A, Fu J, Markwald RR. Study of droplet formation process during drop-on-demand inkjetting of living cell-laden bioink. *Langmuir* 2014;30(30):9130–8.
- [12] Kim E, Baek J. Numerical study on the effects of non-dimensional parameters on drop-on-demand droplet formation dynamics and printability range in the up-scaled model. *Phys Fluids* 2012;24(8):082103.
- [13] Poozesh S, Saito K, Akafuah NK, Graña-Otero J. Comprehensive examination of a new mechanism to produce small droplets in drop-on-demand inkjet technology. *Appl Phys A Mater Sci Process* 2016;122(2):110.
- [14] Pan Y. Heading toward artificial intelligence 2.0. *Engineering* 2016;2(4):409–13.
- [15] Xing EP, Ho Q, Xie P, Wei D. Strategies and principles of distributed machine learning on big data. *Engineering* 2016;2(2):179–95.
- [16] Jia Y, Qi Y, Shang H, Jiang R, Li A. A practical approach to constructing a knowledge graph for cybersecurity. *Engineering* 2018;4(1):53–60.
- [17] Dos Santos EB, Pistor R, Gerlich AP. Pulse profile and metal transfer in pulsed gas metal arc welding: droplet formation, detachment and velocity. *Sci Technol Weld Join* 2017;22(1):1–15.
- [18] Shenfield A, Fleming PJ. Multi-objective evolutionary design of robust controllers on the grid. *Eng Appl Artif Intell* 2014;27(1):17–27.
- [19] Shukri S, Faris H, Aljarah I, Mirjalili S, Abraham A. Evolutionary static and dynamic clustering algorithms based on multi-verse optimizer. *Eng Appl Artif Intell* 2018;72(6):54–66.
- [20] Montonen O, Karmita N, Mäkelä MM. Multiple subgradient descent bundle method for convex nonsmooth multiobjective optimization. *Optimization* 2018;67(1):139–58.
- [21] Shi J, Wu B, Song B, Song J, Li S, Trau D, et al. Learning-based cell injection control for precise drop-on-demand cell printing. *Ann Biomed Eng* 2018;46(9):1267–79.
- [22] Brackbill J, Kothe DB, Zemach C. A continuum method for modeling surface tension. *J Comput Phys* 1992;100(2):335–54.
- [23] Hirt CW, Nichols BD. Volume of fluid (VOF) method for the dynamics of free boundaries. *J Comput Phys* 1981;39(1):201–25.
- [24] Taylor G. The formation of emulsions in definable fields of flow. *P Royal Soc Lond* 1934;146(858):501–23.
- [25] Selmic RR, Lewis FL. Neural-network approximation of piecewise continuous functions: application to friction compensation. *IEEE Trans Neural Netw* 2002;13(3):745–51.
- [26] Sontag ED. Feedback stabilization using two-hidden-layer nets. *IEEE Trans Neural Netw* 1992;3(6):981–90.
- [27] Mostaghim S, Teich J. Strategies for finding good local guides in multiobjective particle swarm optimization (MOPSO). In: *Proceedings of the 2003 IEEE Swarm Intelligence Symposium*; 2003 Apr 26; Indianapolis, IN, USA; 2003.
- [28] Wilppu O, Karmita N, Mäkelä M. New multiple subgradient descent bundle method for nonsmooth multiobjective optimization Report. *Turku Centre for Computer Science, University of Turku*; 2014.
- [29] Kiwiel KC. Proximity control in bundle methods for convex nondifferentiable minimization. *Math Program* 1990;46(1–3):105–22.
- [30] Kingma DP, Ba J. Adam: a method for stochastic optimization 2014. arXiv:1412.6980.
- [31] Yao L, Ge Z. Deep learning of semisupervised process data with hierarchical extreme learning machine and soft sensor application. *IEEE Trans Ind Electron* 2018;65(2):1490–8.
- [32] Ferris CJ, Gilmore KJ, Beirne S, McCallum D, Wallace GG, Panhuis M. Bio-ink for on-demand printing of living cells. *Biomater Sci* 2013;1(2):224–30.